



Contents lists available at ScienceDirect

Journal of Molecular Liquids

journal homepage: [www.elsevier.com/locate/molliq](http://www.elsevier.com/locate/molliq)

# Interfacial behavior of binary, ternary and quaternary oil/water mixtures described from molecular dynamics simulations

Gerard Alonso<sup>a,\*</sup>, Pablo Gamallo<sup>a</sup>, Cristina Rincón<sup>b,c</sup>, Ramón Sayós<sup>a,\*</sup>

<sup>a</sup> Departament de Ciència de Materials i Química Física & Institut de Química Teòrica i Computacional (IQTCUB), Universitat de Barcelona, C. Martí i Franquès 1, 08028 Barcelona, Spain

<sup>b</sup> Repsol Technology Center, Paseo de Extremadura, Km 18, 28935, Móstoles, Madrid, Spain

<sup>c</sup> Department of Structure of Matter, Thermal Physics and Electronics, Universidad Complutense Madrid, Plaza de las Ciencias 1, Ciudad Universitaria, 28040 Madrid, Spain.

## ARTICLE INFO

### Article history:

Received 4 August 2020

Received in revised form 14 October 2020

Accepted 24 October 2020

Available online xxxxx

### Keywords:

Molecular dynamics simulations

Oil/water mixtures

Interfacial tension

Interfacial properties

## ABSTRACT

The correct description of crude oil/water interfaces is a very complex and an important task, particularly to the oil industry, whose main difficulty relies on understanding how the interfacial properties (*i.e.*, interfacial tension and interfacial accumulation) of the system are affected by a very large number of components. To give some additional insight to the oil/water interfacial behavior, eleven oil/water mixtures (*i.e.*, six binary, four ternary and a quaternary mixture) have been modeled through atomistic molecular dynamics simulations at laboratory conditions. All mixtures were built with a model oil based on dodecane, toluene, quinoline and a naphthenic acid, to represent the saturated, aromatic, basic resin and acid resin fractions, respectively.

The results from this contribution show that interfacial tensions can be correlated to interfacial accumulation, which can be used as good starting point in predicting interfacial properties of oil mixtures. Additionally, the interfacial properties of mixtures behave similarly to the most polar pure oil/water interface, while all other compounds stay in the oil bulk as spectators. This behavior raises the question of whether using common n-alkane oils is a good enough approximation for modeling the interfacial properties of crude oils.

© 2020 Elsevier B.V. All rights reserved.

## 1. Introduction

The combustion of fossil fuels is still a major contributor to the worldwide energetic production [1]. However, with primary and secondary oil recovery techniques only one third of the available crude oil can be retrieved from reservoirs [2,3,4]. Different techniques are applied to remove the residual oil. Some examples are the many developments in Enhanced Oil Recovery (EOR) currently available, that encompass gas injection [5], steam flooding [6], fire flooding [7], polymer flooding [8] and surfactant flooding [9], among others. Together with a greater awareness of environmental preservation, many efforts are still carried out to increase our physicochemical knowledge of oil reservoirs, and ultimately to develop better techniques to extract crude oil.

From the literature, it is concluded that oil recovery is improved by increasing the viscosity of the injected water or reducing the viscosity of oil (*i.e.*, in both cases improving the oil/water mobility ratio) [10,11], solving the oil in miscible gases [12] or modifying the oil/rock and oil/water interaction strength through adding different chemicals into the injection water [13,14]. We focus our interest on this latter

technique, whose objective is to reduce the oil/water interfacial tension (IFT) as much as possible and detach the oil from the mineral rocks (*i.e.*, modifying its oil/water/rock contact angle). This has been a common practice in recent experimental studies, where the IFT was reduced by either adding surfactants or nanoparticles [15–21] to the injection water, modifying its pH [22,23], its salinity [22,24,25], or even combining some of them at once [26]. These techniques usually promote a set of polar compounds to accumulate at the oil/water interface to strongly reduce the IFT, sometimes even to ultra-low IFT values (*i.e.*,  $10^{-3}$  mN/m) [27,28], which create oil/water microemulsions. Finally, some of those microemulsions could be stabilized by shielding the droplets *via* electrostatic interactions and preventing droplet coalescence.

Even with such great advancements, there are three reasons that justify a lack of knowledge on the oil/water interfacial behavior: First, the enormous amount of different crude oil compounds; second, the significant variation in pressure, temperature and oil/mineral composition among different reservoirs (or even in the same one) [29]; and third, the severe difficulty in the experimental characterization of oil/water interfaces at a molecular scale. This scenario forced the application of both modeling [30–32], and simulation [33–35], techniques, which have given some alternative insights by analyzing the oil/water interface in presence of additives, such as surfactants [36–38], salts [39,40] or nanoparticles [41]. However, since actual crude oils contain

\* Corresponding authors.

E-mail addresses: [g.alonso@ub.edu](mailto:g.alonso@ub.edu) (G. Alonso), [r.sayos@ub.edu](mailto:r.sayos@ub.edu) (R. Sayós).

countless compounds, these are carried out on very simplified n-alkane oil models [36,37,41], or rarely as mixtures of a limited set of representative compounds [39,42].

With the help of those studies it was concluded that the IFT depends strongly on the oil interfacial concentration, in particular on those species with larger interfacial affinity, who diffuse from the oil bulk to adsorb at the oil interface [43–46]. In fact, many models were developed along the years to relate interfacial properties to the interfacial concentration of species. An example is the one proposed by Eberhart [44], which predicts the IFT of a binary mixture ( $\gamma_{12}^{AVE}$ ) as the average of the pure components IFT ( $\gamma_1, \gamma_2$ ) weighted by its interfacial molar fraction ( $x_1^s, x_2^s$ ), as shown in Eq. (1). This simple model only had an adjustable parameter related to the interfacial accumulation of the component 2 when dissolved in a matrix of component 1 (i.e., component 2 is more interfacially active than component 1). Then, this equation was refined by Laaksonen et al., [47] (Eq. (2) by using interfacial volume fractions ( $\phi_1^s, \phi_2^s$ ), instead of interfacial molar fractions, which allowed to include the effect of molecular size in the interfacial properties.

$$\gamma_{12}^{AVE} = x_1^s \gamma_1 + x_2^s \gamma_2 \quad (1)$$

$$\gamma_{12}^{AVE} = \phi_1^s \gamma_1 + \phi_2^s \gamma_2 \quad (2)$$

These simple ideas have contributed to describe the interfacial phenomena of binary mixtures and can also be applied to understand the complex crude oil behavior. In fact, it is important to fully understand and characterize the interfacial behavior of crude oil as a function of its composition prior to apply any EOR technique. In that sense, molecular simulations can provide significant insight by modeling a multi-component crude oil and characterizing its interfacial behavior with atomic scale resolution and relate the bulk/interfacial fractions to the IFT. Notice, that even though Eqs. (1) or (2) require fitting an empirical parameter to determine the surface affinity of each compound (i.e., to determine  $\phi_i^s$  from the bulk volume fraction), molecular simulations directly account it by modeling the explicit interactions among all species into the simulation cell. So, in this contribution we have employed molecular simulations at laboratory conditions (i.e.,  $T = 300$  K and  $P = 1$  atm) to characterize the correlation among the different interfacial properties (i.e., interfacial tension and interfacial accumulation) in simple and complex model oils as a function of their composition. This correlation can be used as a reasonable starting point to predict the IFT of multicomponent mixtures and to better understand the interfacial behavior of complex model oils.

## 2. Methods and computational details

### 2.1. Model oils

All model oils in this work were built through combination of four species, each one of them from different oil fractions according to the Saturates-Aromatics-Resins-Asphaltenes (SARA) fractionation model. However, to further simplify the complex problem of modeling a crude oil, no compound was chosen to reproduce the behavior of asphaltenes, and only the SAR fractions were considered. The average properties of the saturate and aromatic fractions were reproduced with dodecane and toluene, respectively. On the other hand, two molecules were used to model the resins fraction due to the large chemical variety in this fraction. First, quinoline is used to capture the aromatic/basic behavior of some resins, whereas 3(3-ethylcyclopentyl)propanoic acid (i.e., or simply 3-naphthenic acid) represents the aliphatic/acid part of the fraction. A summary of all the species used to model the simplified crude oil in this work is collected in Fig. 1a.

### 2.2. Molecular dynamics simulations

Force field-based Molecular Dynamics (MD) simulations were carried out using the Large-scale Atomic/Molecular Massively Parallel Simulator (LAMMPS) code [48]. The simulation cell is built as an orthorhombic box with cell parameters  $L_x = L_y = 45$  Å,  $L_z = 200$  Å with periodic boundary conditions imposed in all directions. A region with  $L_x = L_y = 45$  Å,  $L_z = 100$  Å located just in the middle of the simulation cell (i.e., at  $50$  Å  $< z < 150$  Å) is filled with 600–1200 oil molecules depending on its density (See Section S1 in the Supplementary Information for more details). Then, the rest of the simulation cell is filled with 6000 water molecules (i.e., within the regions  $0$  Å  $< z < 50$  Å and  $150$  Å  $< z < 200$  Å). All molecules are initially inserted within their respective regions in random positions and orientations. The resulting setup yields a system with two sensibly long bulk phases of  $L_x = L_y = 45$  Å,  $L_z = 100$  Å initially connected through planar interfaces in the XY plane at  $z = 50$  Å and  $z = 150$  Å (Fig. 1b).

All MD simulations in this work are conducted following the steps of our previous contribution: [36] (i) energy minimization to eliminate molecular overlaps during the random creation of the system, (ii) NVT thermalization to drag the temperature to 300 K using the Langevin thermostat [49] during 50 ps, (iii) NAP<sub>z</sub>T pressure equilibration with the Nosé-Hoover thermostat [50] and Berendsen barostat [51] during 0.5 ns, and (iv) a 30 ns NAP<sub>z</sub>T run with the Nosé-Hoover thermostat and barostat [52] to allow the system to achieve the equilibrium state and extract the average interfacial properties. Notice that NAP<sub>z</sub>T

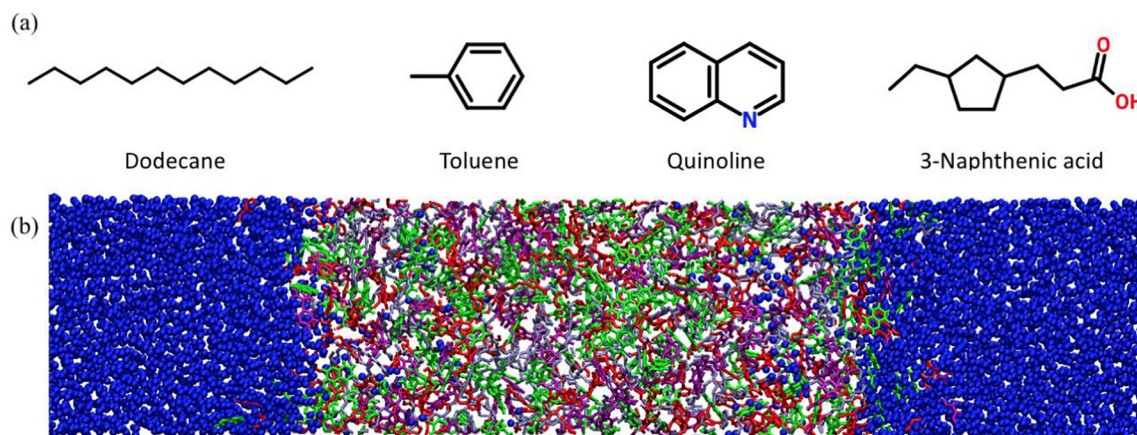


**Fig. 1.** (a) The four molecules used in this work to represent saturates (dodecane), aromatics (toluene) and resins (quinoline and 3-naphthenic acid) in the modeled crude oils, and (b) a typical initial configuration for a Molecular Dynamics oil/water simulation. Black, purple, green, red and blue are dodecane, toluene, quinoline, 3-naphthenic acid and water, respectively.

barostats are only coupled to the z-direction to keep the interfacial area constant during the entire simulation. All simulations are evolved using a timestep of 1 fs with pair interactions calculated using a spherical cut-off of 14 Å and long-range coulombic interactions obtained through the Particle-Particle/Particle-Mesh (PPPM) method [53].

Some simulations (i.e., specially the simulations of mixtures containing very interfacial active components) did not achieve the equilibrium state after 30 ns. The reason is that active species need to diffuse to the interface to reach a real equilibrium state, but instead they formed a metastable aggregate within the bulk phase. These aggregates have significantly long lifetimes that are detected when the bulk density of any component is not constant along the z-direction. In these situations, two extra steps were carried out to equilibrate the system faster: (i) a NVT stage where the working temperature was initially doubled (i.e., from 300 K to 600 K), steadily ramping it down to 300 K during 10 ns, and (ii) a NAP<sub>z</sub>T run at the working temperature and pressure during 10 ns. The first stage increases the kinetic energy of the system through the temperature increase, favoring diffusion processes and the dissolution of metastable aggregates. Finally, the second stage is used to obtain the equilibrium average properties of the system.

### 2.3. Interfacial properties calculation

The interfacial tension of the oil/water systems with  $N = 2$  interfaces was calculated through the integral shown in Eq. (3), also known as Kirkwood and Buff formulation [54]. The three diagonal components of the pressure tensor (i.e.,  $P_n = P_{zz}$  and  $P_t = (P_{xx} + P_{yy})/2$ ) were monitored during the simulation and the resulting IFT values were averaged in time blocks of 0.5 ns. Finally, the equilibrium IFT was obtained by averaging the last 10 ns of the production run.

$$\gamma^{KB} = \int_0^{L_z} [P_n(z) - P_t(z)] dz = \frac{L_z}{N} \left( P_{zz} - \frac{P_{xx} + P_{yy}}{2} \right) \quad (3)$$

However, it is widely known that the interfacial properties, and specially the IFT is very sensitive to the short-range truncation of the potential [55–59]. For this reason, the inhomogeneous long-range corrections (LRCs) for a planar geometry were calculated using as input the equilibrium MD density profiles, as described by Janecek [60]. These density profiles were built dividing the simulation cell along the z-direction in bins of 1 Å width. Then, the number of molecules in each bin is averaged in time blocks of 5 ns, using the last block as the equilibrium density profile. The resulting LRC was then summed to the value obtained in Eq. (3) (i.e., as  $\gamma^{LRC} = \gamma^{KB} + \text{correction}$ ). Uncertainties in the determination of IFTs were obtained by running three replicas of each simulation randomly rotating each molecule to generate different initial states. Then, the uncertainty estimates were taken as the IFT standard deviation in the three replicas.

The molar bulk fraction ( $x_i^b$ ) and the molar interfacial fraction ( $x_i^s$ ) of oil species were also calculated from the equilibrium density profiles. Specifically, those magnitudes are obtained by averaging the density of each compound in the respective bulk and interfacial regions. The oil bulk was defined as the region with dimensions  $L_x = L_y = 45$  Å,  $L_z = 60$  Å in the center of the oil phase where the total density remains constant with an average value  $\langle \rho_o \rangle$ . On the other hand, the interfaces were delimited in the regions where the oil density ( $\rho_o(z)$ ) is larger than zero but lower than  $0.9 \cdot \langle \rho_o \rangle$ . These regions are schematically shown in Fig. 2 for clarity and were labelled as  $z_w^s$  and  $z_o^s$ , which refers to the water and oil side limits of the region, respectively. To select  $z_w^s$  and  $z_o^s$  more accurately, the total oil density ( $\rho_o$ ) was fit to Eq. (4), which uses the common hyperbolic tangent function widely used for interfacial inactive oils (e.g., the profile in Fig. 2a) but also includes a gaussian function per interface to reproduce the interfacial accumulation when needed (e.g., the profile in Fig. 2b).

$$\rho_o(z) = a_L e^{b_L(z-z_{0,L})^2} + a_R e^{b_R(z-z_{0,R})^2} + \frac{\langle \rho_o \rangle}{2} \left[ \tanh\left(\frac{(z-z'_{0,L})}{c_L}\right) - \tanh\left(\frac{(z-z'_{0,R})}{c_R}\right) \right] \quad (4)$$

From Eq. (4),  $\langle \rho_o \rangle$  refers to the previously defined average density of the oil bulk phase;  $a$ ,  $b$  and  $z_0$  are adjustable parameters to capture the shape and position of the left (L) and right (R) gaussian functions; and  $c$  and  $z_0'$  are the fitting parameters to describe the position and stiffness of the left (L) and right (R) hyperbolic tangents. The molar fractions ( $x_i^b$  and  $x_i^s$ ) obtained from the densities in Eq. (4) are converted to volumetric fractions ( $\phi_i^b$  and  $\phi_i^s$ ) assuming ideal mixture behavior.

### 2.4. Force fields

Intermolecular and intramolecular interactions of oil molecules were calculated using the TraPPE-UA force field [61], where bonds were fixed at their equilibrium bond lengths, angles were constrained by a quadratic potential and dihedrals followed a Fourier series expression. To allow the fixed bonds to move, we used the equilibrium spring constants of Amber force field [62] according to the recommendation of TraPPE-UA developers. The TraPPE-EH force field [63] was used, instead of TraPPE-UA, to properly reproduce the quadrupolar moment of aromatic molecules (i.e., toluene and quinoline). This force field was selected because it was explicitly fitted to reproduce the phase equilibrium properties of organic fluids (i.e., densities and cohesive energies), which are critical in the correct description of their interfacial properties. To be completely sure, we have made a preliminary validation step to determine the accuracy of TraPPE force field in reproducing the four components oil/water IFTs at laboratory conditions (i.e.,  $T = 300$  K and  $P = 1$  atm). In that

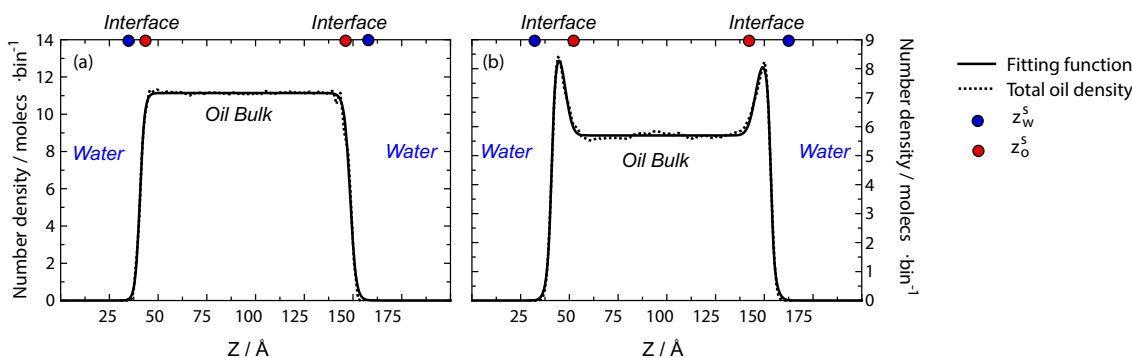


**Fig. 2.** Graphical representation of the defined bulk (yellow) and interfacial (green) regions where the average oil density is calculated. The limits  $z_w^s$  and  $z_o^s$  are represented by blue and red dots, respectively. (a) and (b) show the density profile of interfacial inactive and active oils, respectively.

**Table 1**

Single component oil/water IFT values calculated with five different water models at  $T = 300$  K and  $P = 1$  atm for validation.  $\gamma_i^{KB}$ ,  $\gamma_i^{RC}$  and  $\gamma_i^{exp}$  refer to the uncorrected, long-range corrected and reference experimental values, respectively. The Ref. column details the original works, where experimental values were obtained.

System	Water Model	$\gamma_i^{KB} / \text{mN} \cdot \text{m}^{-1}$	$\gamma_i^{RC} / \text{mN} \cdot \text{m}^{-1}$	$\gamma_i^{exp} / \text{mN} \cdot \text{m}^{-1}$	Ref.
Dodecane/ $\text{H}_2\text{O}$	SPC	$48.1 \pm 0.7$	$48.2 \pm 0.7$		
	SPC/E	$54.3 \pm 0.5$	$54.3 \pm 0.5$	51.0	70
	TIP3P	$56.0 \pm 0.4$	$56.0 \pm 0.4$	52.3	71
	TIP4P	$48.6 \pm 0.7$	$48.6 \pm 0.7$		
	TIP4P/2005	$52.2 \pm 0.5$	$51.9 \pm 0.5$		
Toluene/ $\text{H}_2\text{O}$	SPC	$41.7 \pm 0.3$	$42.0 \pm 0.3$		
	SPC/E	$47.3 \pm 0.4$	$49.4 \pm 0.4$	36.0	73
	TIP3P	$48.9 \pm 0.4$	$51.0 \pm 0.4$	36.1	74
	TIP4P	$42.2 \pm 0.3$	$44.4 \pm 0.3$		
	TIP4P/2005	$47.7 \pm 0.4$	$49.3 \pm 0.4$		
Quinoline/ $\text{H}_2\text{O}$	SPC	$31.1 \pm 1.6$	$32.0 \pm 1.6$		
	SPC/E	$33.5 \pm 1.5$	$34.3 \pm 1.5$		
	TIP3P	$35.6 \pm 1.5$	$36.4 \pm 1.5$	33.0	72
	TIP4P	$28.7 \pm 1.7$	$29.5 \pm 1.7$		
	TIP4P/2005	$29.5 \pm 1.7$	$30.0 \pm 1.7$		
3-Napht. acid/ $\text{H}_2\text{O}$	SPC	$16.5 \pm 0.4$	$17.1 \pm 0.4$		
	SPC/E	$20.4 \pm 1.1$	$21.0 \pm 1.1$		
	TIP3P	$25.0 \pm 2.0$	$25.6 \pm 2.0$	11.0–13.0	72
	TIP4P	$20.1 \pm 1.1$	$20.7 \pm 1.1$		
	TIP4P/2005	$20.6 \pm 1.2$	$20.9 \pm 1.2$		

validation, we have also tested some of the most popular non-polarizable water force fields (*i.e.*, SPC [64], SPC/E [65], TIP3P [66], TIP4P [67] and TIP4P/2005 [68], with geometries constrained with the SHAKE algorithm [69]). Finally, standard Lorentz-Berthelot combining rules were used to determine the parameters for unlike Lennard-Jones intermolecular interactions ( $\epsilon_{ij}$ ,  $\sigma_{ij}$ ).

The results of this validation are compiled in Table 1, where it is seen that all TraPPE/water model combinations provide a similar equilibrium IFT value. This fact shows that the TraPPE force field is capable of capturing the fundamental cohesive energy of the organic species, regardless of the water model. In general, all water models give reasonable results (*i.e.*, deviations of less than 5 mN/m) for the dodecane/water and quinoline/water IFTs [70–72], being TIP3P and TIP4P the force fields that exhibit the larger average deviations and SPC, SPC/E and TIP4P/2005 the better agreement. However, all force fields overestimate the toluene/water and 3-naphthenic acid/water IFTs, according to the available experimental results [72–74]. In these systems, SPC and TIP4P give the best agreement, followed by TIP4P/2005, SPC/E and finally, TIP3P. To conclude, TIP3P is the water force field that exhibits larger deviations with experimental data for the oil components tested in this work. TIP4P, TIP4P/2005 and SPC/E give good results for some oils but a worse interfacial representation in others. Finally, SPC seems to be the most adequate water force field to reproduce liquid/liquid interfacial properties of the selected compounds because it exhibits the lowest deviation with respect to the reported experiments. Additionally, as a three-point model, SPC is also one of the best computationally efficient models available in atomistic molecular representations to model oil/

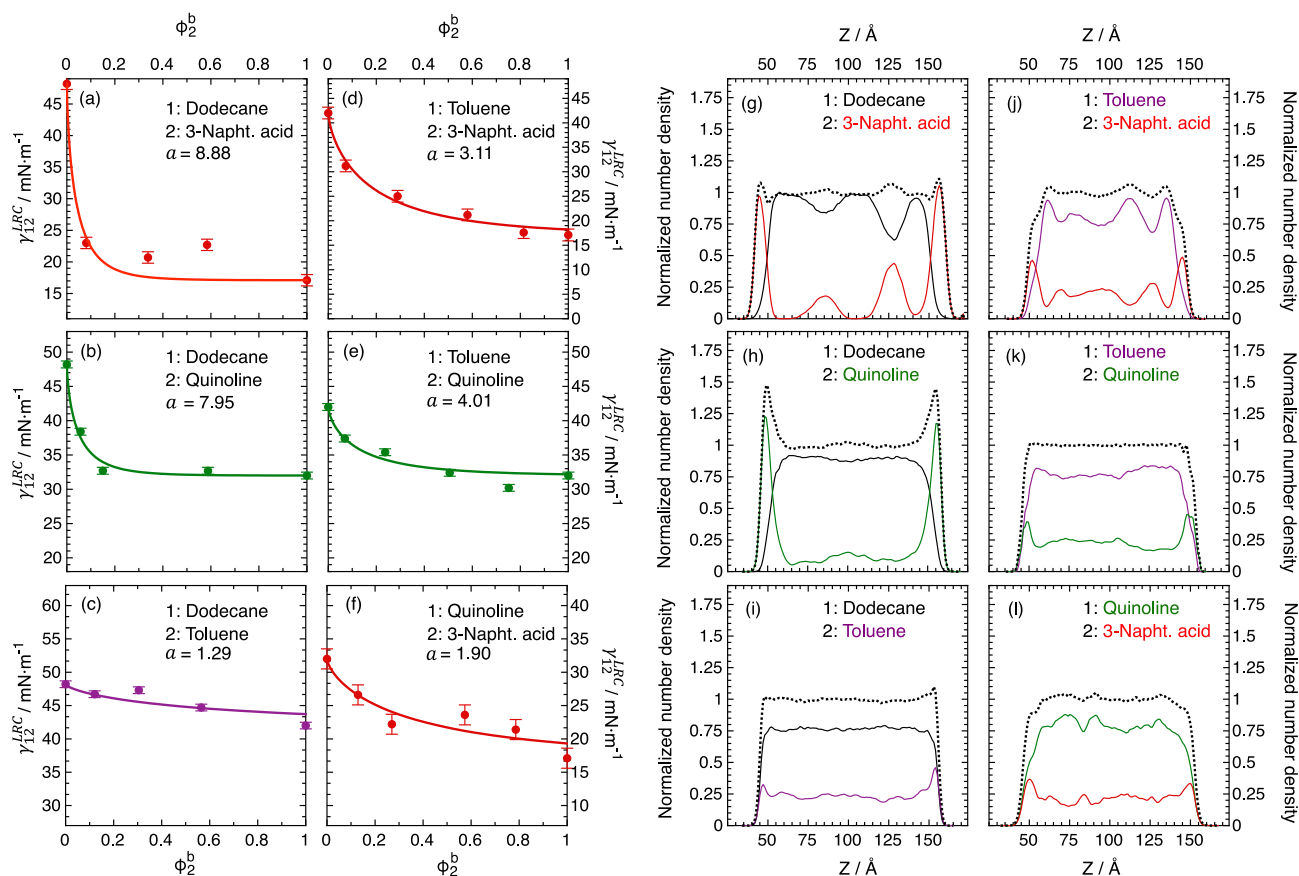


**Fig. 3.** (a–f) Calculated oil/water IFT of the six binary mixtures plotted against its equilibrium bulk volume fraction ( $\phi_2^b$ ). The  $\alpha$  value corresponds to the adjustable parameter in the IFT correlation for binary mixtures of Kim et al. [77]:  $\gamma_{12} = (\gamma_1 - \gamma_2)e^{-\alpha\phi_2^b} - \gamma_2$ . (g–l) Oil-centered equilibrium  $z$ -distributions of the six binary mixtures containing an initial molar fraction of  $x_2^b = 0.25$ . Solid black, purple, green and red lines correspond to dodecane, toluene, quinoline and 3-naphthenic acid, respectively. Dotted lines indicate the total oil distribution. MD conditions:  $T = 300$  K,  $P = 1$  atm.



water interfaces. For this reason, SPC is the water model finally selected to develop this work.

Notice that regardless of the water force field selected, the toluene/water IFT is overestimated by TraPPE-EH by at least 6.0 mN/m, and TraPPE-UA overestimates the 3-naphthenic acid/water IFT by 4.1 mN/m. These differences are not very large, but their deviations as pure compounds can be magnified in their interfacial mixture behavior. Some authors have dealt with this issue by adding an oil/water interaction parameter ( $k_{ij}$ ) in their simulations to fit the obtained properties to experimental results [75,76]. However, the aim of this work is to predict interfacial properties of oils and their mixtures, so this practice was not considered.

### 3. Results and discussion

#### 3.1. Oil binary mixtures

First, we have studied the variation of oil/water IFT with the composition of the six possible binary combinations at laboratory conditions (i.e.,  $T = 300$  K and  $P = 1$  atm). We define the species 1 and 2 as the least and most interfacial active species at the oil/water interface, respectively. The results are shown in Fig. 3a–f, where it can be seen a decrease of the IFT when increasing the volume fraction of component 2 in the mixture. This decrease follows a negative deviation from ideality because polar components migrate preferentially to the interface reducing

the IFT below the ideal average. This deviation is larger for binary mixtures with high maximum interfacial pressure ( $\pi_{max}$ ), which is known as the IFT difference between the two pure oil/water interfaces conforming the mixture ( $\pi_{max} = |\gamma_1^{LR} - \gamma_2^{LR}|$ ). For example, in Fig. 3a the dodecane ( $\gamma_1^{LR} = 48.2$  mN/m) is mixed with 3-naphthenic acid ( $\gamma_2^{LR} = 17.1$  mN/m), which has a  $\pi_{max} = 31.1$  mN/m and a very sharp slope. However, in Fig. 3c the same dodecane is mixed with toluene ( $\gamma_2^{LR} = 42.0$  mN/m), which has a  $\pi_{max} = 6.2$  mN/m and a less pronounced pattern. It is important to consider that if active species migrate from bulk to interfaces, all bulk volume fractions will change at equilibrium. For this reason, all calculations in Fig. 3a–f already show the IFT values vs. the equilibrium bulk volume fraction instead. Finally, all the calculated IFTs were fitted to the empirical equation of Kim et al., [77] to provide the interpolated and smoothed IFT pattern from the MD simulations.

From this information one can start to infer the interfacial affinity of each species to the water interface. Essentially, two groups can be distinguished: (i) the less polar block formed by dodecane and toluene and (ii) the polar block with quinoline and 3-naphthenic acid. Dodecane and toluene both exhibit a similar and low interfacial activity (i.e., toluene is slightly more active than dodecane), so in their mixture, the IFT decreases almost linearly with toluene volume fraction. This is also the case when mixing quinoline with 3-naphthenic acid, where both exhibit a high, but similar, interfacial activity and the IFT again decreases almost linearly. However, when a molecule of group (i) is mixed with another one of group (ii) the difference in interfacial activity makes the polar compounds to migrate significantly to the interface, relegating the other components to the bulk. In this situation the IFT of the mixture decreases sharply from the pure  $\gamma_1^{LR}$  value. To conclude, the interfacial activity of the four compounds according to Fig. 3a–f is 3-naphthenic acid > quinoline > toluene > dodecane.

To illustrate this phenomenon, Fig. 3g–l compiles the density profiles for each compound in each binary mixture (i.e., a single profile for each mixture is shown, with initial bulk molar fraction  $x_2^b \approx 0.25$ , which is not the equilibrium  $\phi_2^b$ ). The profiles containing dodecane (Fig. 3g–i) are related to the second point in the IFT plots of Fig. 3a–c, whereas the rest (Fig. 3j–l) corresponds to the third point in the IFT plots of Fig. 3d–f. These density profiles have been normalized with the average density of the bulk phase so that  $\langle \rho \rangle_{tot}^b = 1$ . In Fig. 3g–h one can see that either the 3-naphthenic acid and quinoline have abandoned significantly the bulk phase to accumulate very strongly into the oil/water interface (i.e., their bulk density is very small at equilibrium). In those examples, the acid has saturated the interface and started to form some aggregates

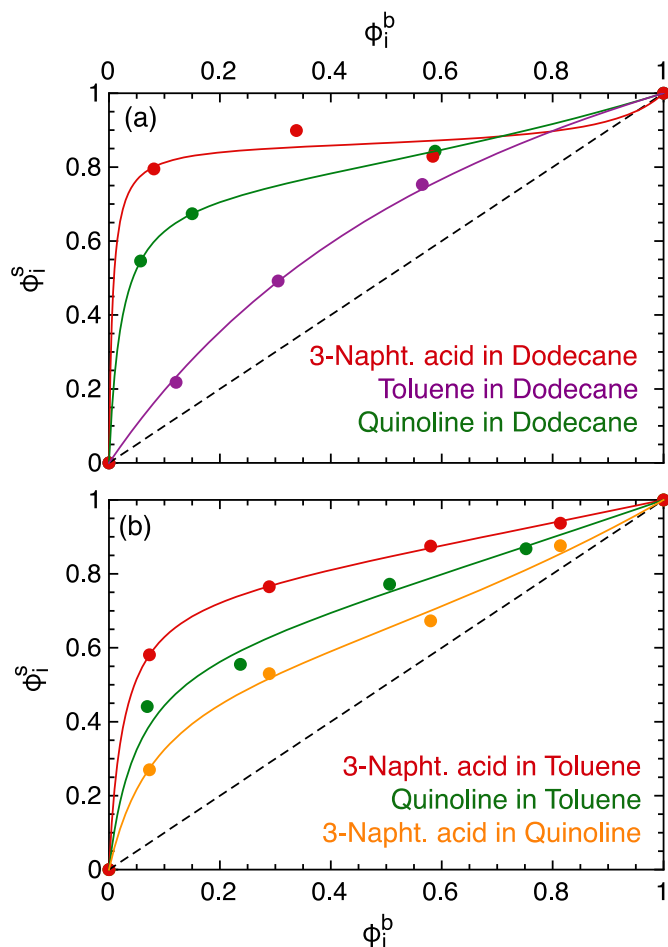


**Fig. 4.** Interfacial vs bulk volume fractions of polar components in oil binary mixtures. Dots correspond to MD results and solid lines are just a guide to the eye. The dashed line corresponds to an equal interfacial and bulk volume fractions. MD conditions:  $T = 300$  K,  $P = 1$  atm.

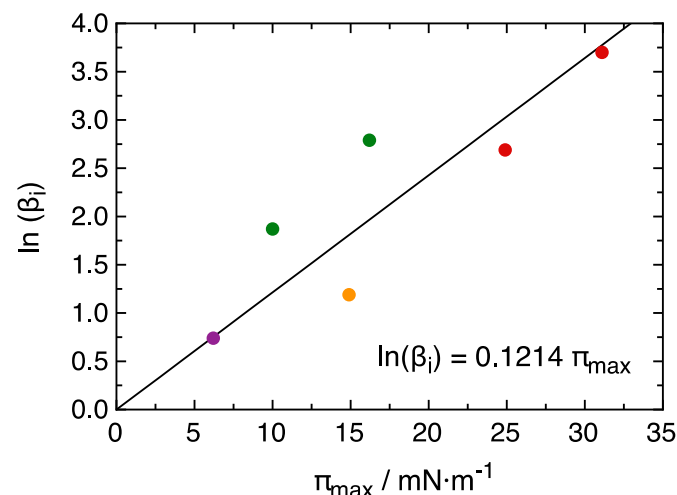


**Fig. 5.** Linear correlation between low-concentration Langmuir equilibrium constants vs.  $\pi_{max}$  for the tested binary mixtures. MD conditions:  $T = 300$  K,  $P = 1$  atm.

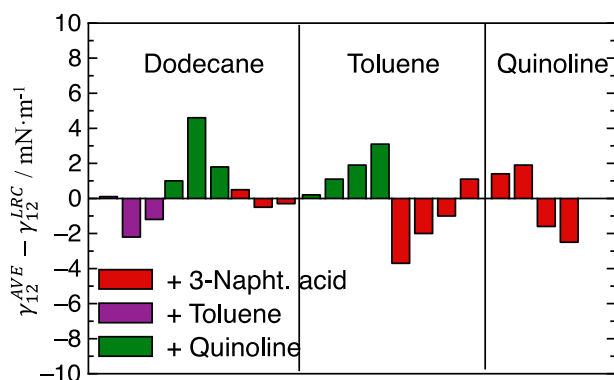


**Fig. 6.** Deviation between the MD calculated interfacial tension values ( $\gamma_{12}^{LRC}$ ) and the average  $\gamma_{12}^{AVE} = \phi_1^s \gamma_1 + \phi_2^s \gamma_2$  obtained from the z-distributions. MD conditions:  $T = 300$  K,  $P = 1$  atm.

into the oil bulk due to their surfactant-like structure (i.e., a polar COOH head and a non-polar C2-CP-C2 tail). Notice that these aggregates could not be removed through a thermal cycle to break meta-stable aggregates (i.e.,  $300\text{ K} \rightarrow 600\text{ K} \rightarrow 300\text{ K}$ ; see Section 2.2. Molecular dynamics simulations), which ensures that the systems are correctly equilibrated. Otherwise, quinoline still have not saturated the interface completely. This is inferred from Fig. 3a–b where the dodecane + acid mixture achieved an IFT plateau, whereas the dodecane + quinoline mixture did not. The interfacial density in all other mixtures (Fig. 3i–l) is relatively similar to their bulk density, so the IFT deviates less from the ideal linear behavior.

Those density profiles have also been used to quantify the interfacial volume fraction of each component in the mixtures. As seen in Fig. 3g–l, when a species accumulates at the oil/water interface, it migrates from the bulk to the interface (i.e., and thus  $\phi_2^s > \phi_2^b$ ), while displacing the other species from the bulk to the interface (i.e., and thus  $\phi_1^b > \phi_1^s$ ). According to that definition, Fig. 4 shows the interfacial volume fraction of component 2 as a function of its bulk volume fraction for each binary mixture. The results quantify that 3-naphthenic acid has the strongest interfacial accumulation at low volume fractions when dissolved into low polarity oils such as dodecane or toluene. This behavior is expected, considering that 3-naphthenic acid contains a polar COOH group that can interact favorably with water via electrostatic, dipole and hydrogen-bond interactions, while neither toluene nor dodecane have strong attractive interactions with water. Also, when dissolved into a polar oil such as quinoline, 3-naphthenic acid is still exhibiting a mild interfacial accumulation. This might be due to its surfactant-like structure, which also contributes to its strong interfacial affinity. On the other hand, quinoline migrates less than 3-naphthenic acid to interfaces

**Table 2**

MD IFT results ( $\gamma^{LRC}$ ) and volumetric bulk/interfacial volume fractions of all species for the higher order mixtures studied at  $T = 300$  K and  $P = 1$  atm. The  $\gamma^{AVE}$  column refers to the direct interfacial volume average using the MD  $\phi_i^s$  values and the  $\gamma^{PRE}$  column corresponds to the same average with the  $\phi_i^{s, PRE}$  predicted via Eq. (6).

Dodecane		Toluene		Quinoline		3-Napht. acid		IFT / $\text{mN} \cdot \text{m}^{-1}$		
$\phi_1^b$	$\phi_1^s$	$\phi_1^b$	$\phi_1^s$	$\phi_1^b$	$\phi_1^s$	$\phi_1^b$	$\phi_1^s$	$\gamma^{LRC}$	$\gamma^{AVE}$	$\gamma^{PRE}$
0.64	0.25	0.24	0.20	0.12	0.55	–	–	$34.8 \pm 0.2$	38.1	39.9
0.75	0.36	0.16	0.14	0.09	0.50	–	–	$37.7 \pm 0.8$	39.2	41.0
0.57	0.02	0.23	0.05	–	–	0.20	0.93	$20.5 \pm 1.1$	18.9	20.1
0.76	0.09	0.16	0.05	–	–	0.08	0.86	$22.8 \pm 1.4$	21.3	23.8
0.58	0.09	–	–	0.25	0.26	0.17	0.65	$23.2 \pm 1.6$	23.8	21.8
0.77	0.09	–	–	0.14	0.22	0.09	0.69	$21.9 \pm 0.9$	23.1	24.0
–	–	0.30	0.12	0.31	0.27	0.39	0.61	$23.9 \pm 0.5$	24.1	19.6
–	–	0.70	0.31	0.15	0.16	0.15	0.53	$28.7 \pm 1.1$	27.2	22.9
0.41	0.02	0.18	0.04	0.21	0.19	0.20	0.75	$23.8 \pm 1.6$	21.6	21.1

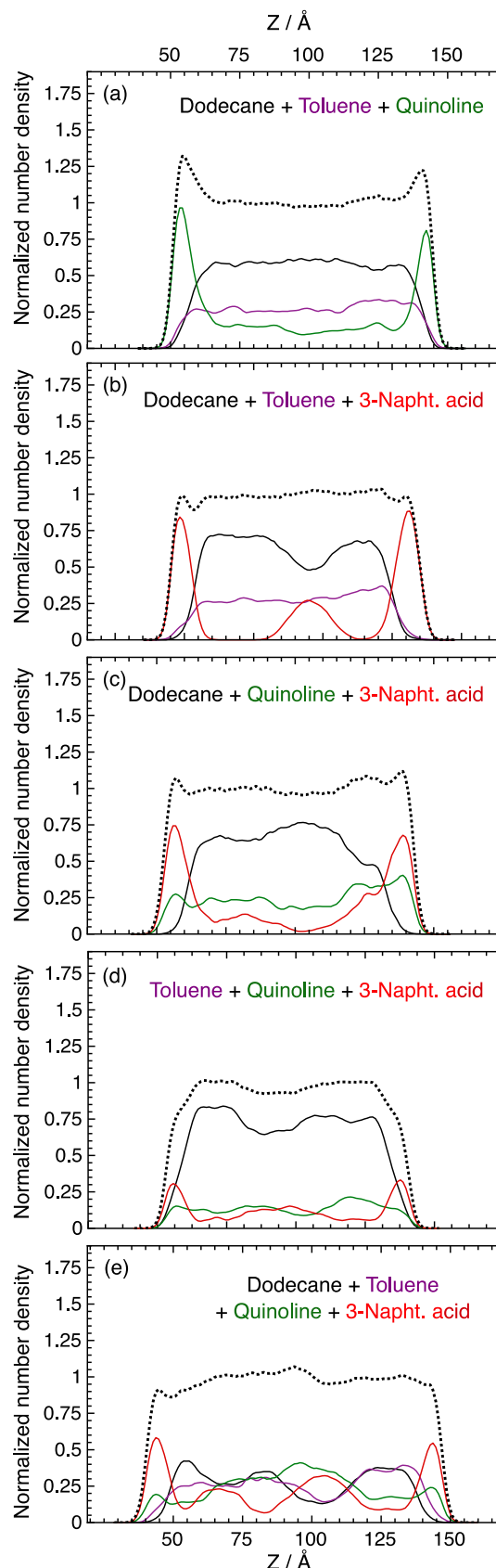


**Fig. 7.** (a–d) Oil-centered equilibrium z-distributions of the four ternary mixtures containing an initial molar fraction of  $x_1^b = 0.50$  and  $x_2^b = x_3^b = 0.25$  and (e) z-distributions of the quaternary mixture with an initial molar fraction of  $x_1^b = x_2^b = x_3^b = x_4^b = 0.25$ . Dotted lines indicate the total oil distribution. MD conditions:  $T = 300$  K,  $P = 1$  atm.

because it is only attracted to water through the aforementioned molecular interactions, but it does not have a surfactant-like structure. Finally, toluene only accumulates slightly at the interface when mixed with dodecane because it can interact with water through the aromatic quadrupolar interactions. To conclude, the interfacial activity of the four species is definitely ranked as 3-naphthenic acid > quinoline > toluene > dodecane.

This ranking inversely follows the pure oil/water IFT values seen in Table 1, which is also related to the strength of oil/water adhesive interactions. Additionally, the  $\phi_2^s$  vs  $\phi_2^b$  slopes at low volume fraction shown in Fig. 4 can be correlated to the maximum interfacial pressure of the binary mixture (i.e.,  $\pi_{max}$ ). To quantify this correlation, we have assumed that at low volume fractions (i.e., approximately at  $\phi_2^b < 0.35$ ) the interfacial adsorption of component 2 ( $\phi_2^s$ ) can be approximated by a Langmuir expression [78] (Eq. (5)), as shown by other authors [79,46]. Notice that Eq. (5) holds over the whole concentration range in such a way that  $\phi_i^s \rightarrow 1$  when  $\phi_i^b \rightarrow 1$  and  $\phi_i^s \rightarrow 0$  when  $\phi_i^b \rightarrow 0$ . Also, the Langmuir-like behavior is reproduced only at diluted solutions, whereas it changes to a linear pattern at higher component 2 content. Then, we have fitted these low volume fraction results of Fig. 4 to Eq. (5) to obtain the Langmuir equilibrium constant ( $\beta_i$ ). Finally, we have shown in Fig. 5 a linear trend between the  $\pi_{max}$  and  $\ln(\beta_i)$  in the studied binary mixtures.

$$\phi_i^s = \frac{\beta_i \phi_i^b}{1 + \beta_i \phi_i^b - \phi_i^b} \quad (5)$$

After describing the binary interfacial behavior for all mixtures, we have also obtained their IFT with the assumption of Laaksonen et al. [47] (i.e., by averaging their single component oil/water  $\gamma_i^{RC}$  weighted by the MD calculated interfacial volume fraction  $\phi_i^s$  as described in Eq. (2)). Then, we have compared those values with the  $\gamma_{12}^{RC}$ , calculated by the pressure tensor method, obtaining a good agreement among

both methods in the range of  $0.1 \text{ mN/m} \leq |\Delta\gamma| \leq 4.5 \text{ mN/m}$ , as it can be seen in Fig. 6. This corresponds to an average deviation of  $|\Delta\gamma| = 1.6 \text{ mN/m}$  (i.e., 5.6%), which further validates the assumption made by Laaksonen et al. [47] for these kinds of mixtures.

### 3.2. Higher order oil mixtures

After the thorough analysis of the oil binary mixtures, the insight gained has been applied to describe the five higher order mixtures (four ternary and one quaternary). A similar process has been employed in which the IFT of mixtures with different composition was analysed through MD simulations. Then, the z-distributions of each component within each mixture was obtained to calculate each bulk and interfacial equilibrium volume fractions. Finally, we have compared the  $\gamma^{RC}$  with the  $\gamma^{AVE}$  values. Note that  $\gamma^{AVE}$  is calculated with the extension of Eq. (2) to three and four components. Moreover, from Fig. 5 we have inferred that the interfacial accumulation of species can be correlated to the IFT of the pure components involved in the mixture. For this reason, we have also predicted the interfacial volume fractions ( $\phi_i^{s,PRE}$ ) of ternary and quaternary mixtures by applying the multicomponent Langmuir isotherm (Eq. (6)). Similarly, to Eq. (5), this expression can only be ideally applied at a low interfacial active component volume fractions. Once all  $\phi_i^{s,PRE}$  values are calculated, the IFT is predicted through Eq. (2), equivalently to  $\gamma^{AVE}$ . However, since those values were obtained by predicted interfacial volume fractions, we have defined it as  $\gamma^{PRE}$ .

$$\phi_i^{s,PRE} = \frac{\beta_i \phi_i^b}{1 + \sum_j \beta_j \phi_j^b - \phi_j^b} \text{ with } \beta_i = e^{0.1214 (\gamma_1^{RC} - \gamma_i^{RC})} \quad (6)$$

The MD calculated IFTs and the bulk and interfacial volume fractions are compiled in Table 2. From the ratio between the  $\phi_i^b$  and  $\phi_i^s$  we can

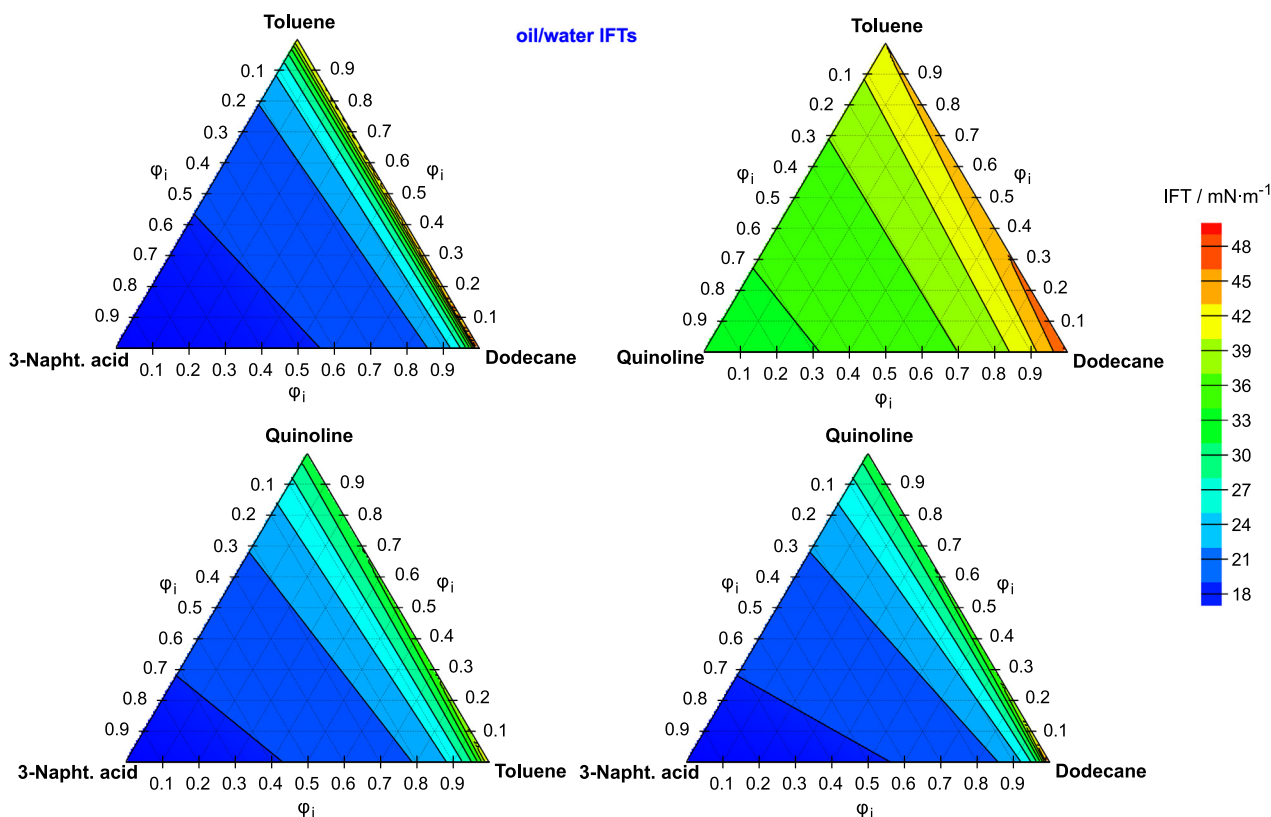


Fig. 8. Predicted oil/water IFT vs. bulk volume fraction ternary diagrams built with the combination of Eq. (2) and Eq. (6). Valid for laboratory conditions:  $T = 300 \text{ K}$ ,  $P = 1 \text{ atm}$ .

infer the interfacial activity of each species within the mixtures. Following a similar trend than in the binary systems, mixtures containing dodecane + toluene + a polar compound (*i.e.*, either quinoline or 3-naphtheneic acid) exhibit an interfacial depletion ( $\phi_i^b > \phi_i^s$ ) of both non-polar species and a polar compound accumulation ( $\phi_i^s > \phi_i^b$ ). The acid is again showing a higher interfacial affinity than quinoline in ternary mixtures, as revealed by its large  $\phi_i^s > 0.85$  values even at  $\phi_i^b < 0.10$ . On the other hand, ternary mixtures containing only one non-polar compound (*i.e.*, either dodecane or toluene) and both quinoline + 3-naphtheneic acid show only interfacial depletion of the non-polar compound. Both polar species compete for the interface, so the activity of 3-naphtheneic acid is slightly reduced to allow some quinoline to occupy the interfacial region, who exhibits a  $\phi_i^b \approx \phi_i^s$ . This behavior can also be seen in Fig. 7 for some of the mixtures. In particular, Fig. 7a-b show very large interfacial density peaks denoting total accumulation of quinoline and 3-naphtheneic acid, while from Fig. 7c-e those peaks are smaller due to competition of both polar components.

Table 2 also includes the interfacial averaged  $\gamma^{AVE}$  and predicted  $\gamma^{PRE}$  values. The results show a good agreement between the two IFT values in almost all of the simulated mixtures, extending the validity of the correlation deduced from binary to ternary and even quaternary mixtures. From this information we can infer that a good first approximation of the interfacial accumulation and interfacial tension of any diluted higher order mixture can be deduced from the correlated Langmuir constants of binary mixtures. After this validation, we have plotted the predicted  $\gamma^{PRE}$  values for each ternary mixture as a function of their composition in a heatmap (Fig. 8). This information provides an estimate of the oil/water interfacial behavior of all possible ternary mixtures that can be built with the four studied components.

## 4. Conclusions

We have successfully determined the interfacial properties (*i.e.*, IFT and interfacial accumulation) of oil binary, ternary and quaternary mixtures with pure water by using molecular dynamics simulations. Specifically, dodecane, toluene, quinoline and 3-naphtheneic acid were used as a simple model for saturates, aromatics and resins of standard model crude oils.

The main results indicate that there is a correlation between the interfacial accumulation and the pure oil/water IFT of each component in a mixture. This correlation occurs because there is a competition among all molecules to occupy the interface, where the most polar components (*i.e.*, with stronger water affinity and lower pure oil/water IFT) will accumulate more than the others (*i.e.*, with weaker water affinity and higher pure oil/water IFT). Then, since the interfacial occupation is a competitive process, it depends on the polarity and the IFT of all components in the mixture. This framework allowed us to describe a correlation, that coupled to a Langmuir isotherm, gives a good predictive estimate of both the interfacial volume fraction and the interfacial tension of binary and higher order mixtures by only using the four pure oil/water IFT values.

Finally, the interfacial properties in all of the studied mixtures were dominated by 3-naphtheneic acid and quinoline, species that diffuse to the interface and exhibit the strongest interfacial contribution. This fact implies that saturates and aromatic components should play a spectator role in determining the physicochemical properties of oil/water interfaces. For this reason, chemical EOR efforts should be focused on the interactions of water with these polar compounds. The obtained results also question the adequacy of using non-polar oils such as n-alkanes as a model crude oil when evaluating its interfacial properties for chemical EOR, instead of a possibly more realistic organic acid/water interface.

## Author statement

### Gerard Alonso

He has carried out all the calculations and their analysis and wrote the manuscript along with Ramón Sayós.

### Cristina Rincón

She has supervised a part of the calculations (from REPSOL company) and also revised the manuscript.

### Pablo Gamallo

He was the codirector of Gerard Alonso PhD thesis. He supervised all Gerard's work and revised the manuscript.

### Ramón Sayós

He was the director of Gerard Alonso PhD thesis. He supervised all Gerard's work and wrote the manuscript along with Gerard Alonso.

## Declaration of Competing Interest

The authors have no competing of interests to declare.

## Acknowledgments

Financial support to this research has been provided from the Spanish Ministry of Science, Innovation and Universities with project and post-doctoral grants RTI2018-094757-B-I00, MCIU/AEI/FEDER, UE and MDM-2017-0767, and the Generalitat de Catalunya for 2017SGR13 and XRTQC projects. PG specially thanks his Serra Hünter Associate Professorship to the Generalitat de Catalunya.

## References

- [1] V. Smil, *Energy Transitions: Global and National Perspectives*, Praeger, Santa Barbara, 2016.
- [2] A. Agi, R. Junin, M.F. Syamsul, A.S. Chong, A. Gbadamosi, Intermittent and short duration ultrasound in a simulated porous medium, *Petroleum* 5 (2018) 42–51.
- [3] A.O. Gbadamosi, J. Kiwalabye, R. Junin, A. Augustine, A review of gas enhanced oil recovery schemes used in the North Sea, *J. Pet. Explor. Prod. Technol.* 5 (2018) 1–15.
- [4] A. Muggeridge, A. Cockin, K. Webb, H. Frampton, I. Collings, T. Moulds, P. Salino, Recovery rates, enhanced oil recovery and technological limits, *Philosophical Transactions of the Royal Society A* 372 (2014) 20120320 In this issue.
- [5] L. Lin, Z. Yang, X. Liu, J. Sun, Y. He, H. Guo, Experiments on the permeability limits of tight oil reservoirs for gas flood recovery, *Spec. Top. Rev. Porous Media Int. J.* 7 (2016) 385–390.
- [6] A. Mollaei, B. Maini, Steam flooding of naturally fractured reservoirs: basic concepts and recovery mechanisms, *J. Can. Pet. Technol.* 49 (2010) 65–70.
- [7] E. Mokheimer, M. Hamdy, Z. Abubakar, R. Shakeel, M.A. Habib, M. Mahmoud, A comprehensive review of thermal enhanced oil recovery: Techniques evaluation, *J. Energy Resour. Technol.* 141 (2019) 030801:1–18.
- [8] H. Saboorian-Jooybari, M. Dejam, Z. Chen, Heavy oil polymer flooding from laboratory core floods to pilot tests and field applications: half-century studies, *J. Pet. Sci. Eng.* 142 (2016) 85–100.
- [9] S. Kumar, A. Mandal, Studies on interfacial behavior and wettability change phenomena by ionic and nonionic surfactants in presence of alkalis and salt for enhanced oil recovery, *Appl. Surf. Sci.* 372 (2016) 42–51.
- [10] M.S. Kamal, A.S. Sultan, U.A. Al-Mubaiyeh, I.A. Hussein, Review on polymer flooding: rheology, adsorption, stability, and field applications of various polymer systems, *Polym. Rev.* 55 (2015) 491–530.
- [11] M.S. Kamal, A.S. Sultan, U.A. Al-Mubaiyeh, I.A. Hussein, Y. Feng, Rheological properties of thermoviscosifying polymers in high-temperature and high-salinity environments, *Can. J. Chem. Eng.* 93 (2015) 1194–1200.
- [12] H.R. Lashgari, A. Sun, T. Zhang, G.A. Pope, L.W. Lake, Evaluation of carbon dioxide storage and miscible gas EOR in shale oil reservoirs, *Fuel* 241 (2019) 1223–1235.
- [13] A.A. Umar, I.B.M. Saaid, A.A. Sulaimon, R.B.M. Pilus, A review of petroleum emulsions and recent progress on water-in-crude oil emulsions stabilized by natural surfactants and solids, *J. Pet. Sci. Eng.* 165 (2018) 673–690.
- [14] S.O. Olayiwola, M. Dejam, A comprehensive review on interaction of nanoparticles with low salinity water and surfactant for enhanced oil recovery in sandstone and carbonate reservoirs, *Fuel* 241 (2019) 1045–1057.
- [15] M.S. Kamal, I.A. Hussein, A.S. Sultan, Review on surfactant flooding: phase behavior, retention, IFT, and field applications, *Energy Fuel* 31 (2017) 7701–7720.
- [16] H. Aziz, S.Q. Tunio, Enhancing oil recovery using nanoparticles—a review, *Adv. Nat. Sci. Nanosci. Nanotechnol.* 10 (2019) 03300:1–12.
- [17] M.S. Kamal, S.M.S. Hussain, L.T. Fogang, A zwitterionic surfactant bearing unsaturated tail for enhanced oil recovery in high-temperature high-salinity reservoirs, *J. Surfactant Deterg.* 21 (2018) 165–174.
- [18] Y. Li, W. Zhang, B. Kong, M. Puerto, B.O. Xinning, Z.S. Sha, Y. Yang, Y. Liu, G. Songyuan, C. Miller, G.J. Hirasaki, Mixtures of anionic/cationic surfactants: a new approach for enhanced oil recovery in low-salinity, high-temperature sandstone reservoir, *SPE J.* 21 (2016) 1164–1177.
- [19] L.J. Giraldo, J. Gallego, J.P. Villegas, C.A. Franco, F.B. Cortés, Enhanced waterflooding with NiO/SiO<sub>2</sub> 0-D Janus nanoparticles at low concentration, *J. Pet. Sci. Eng.* 174 (2019) 40–48.



- [20] C. Hu, Y. Zhang, Z. Yang, Z. Zhang, H. Fan, Q. You, Experimental study on functional characteristics of pH-sensitive nanoparticles for pressure reduction and augmented injection in tight oil reservoir, *J. Mol. Liq.* 311 (2020) 113253:1–9.
- [21] M.S. Alnarabiji, M.M. Husein, Application of bare nanoparticle-based nanofluids in enhanced oil recovery, *Fuel* 267 (2020) 117262:1–12.
- [22] B. Honarvara, A. Rahimia, M. Safarib, S. Rezaee, M. Karimia, Favorable attributes of low salinity water aided alkaline on crude oil-brinecarbonate rock system, *Colloid. Surface. A* 585 (2020) 124144:1–12.
- [23] Y. Chen, Q. Xie, W. Pu, A. Saeedi, Drivers of pH increase and implications for low salinity effect in sandstone, *Fuel* 218 (2018) 112–117.
- [24] A.A. Costa, J. Trivedi, J. Soares, P. Rocha, G. Costa, Marcelo Embiruçu, An experimental evaluation of low salinity water mechanisms in a typical Brazilian sandstone and light crude oil with low acid/basic number, *Fuel* 273 (2018) 117694:1–18.
- [25] P. Rostamia, M.F. Mehrabani, M. Sharifia, M. Dejamb, S. Ayatollahi, Effect of water salinity on oil/brine interfacial behaviour during low salinity waterflooding: a mechanistic study, *Petroleum* 5 (2019) 367–374.
- [26] A.O. Gbadamosi, R. Junin, M.A. Manan, A. Agi, A.S. Yusuf, An overview of chemical enhanced oil recovery: recent advances and prospects, *Int. Nano Lett.* 9 (2019) 171–202.
- [27] N. Pal, N. Saxena, A. Mandal, Phase behavior, Solubilization, and phase transition of a microemulsion system stabilized by a novel surfactant synthesized from castor oil, *J. Chem. Eng. Data* 62 (2017) 1278–1291.
- [28] A. Mandal, S. Kar, A thermodynamic assessment of micellization for a mixture of sodium dodecyl benzene sulfonate and tween 80 surfactants for ultralow interfacial tension, *Fluid Phase Equilib.* 408 (2016) 212–222.
- [29] B. Tissot, D. Welte, *Petroleum Formation and Occurrence*, Springer, Berlin, 1978.
- [30] X. Zhou, Q. Yuan, Y. Zhang, H. Wang, F. Zeng, L. Zhang, Performance evaluation of CO<sub>2</sub> flooding process in tight oil reservoir via experimental and numerical simulation studies, *Fuel* 236 (2019) 730–746.
- [31] M.J. Blunt, B. Bijeljic, H. Dong, O. Gharbi, S. Iglauer, P. Mostaghimi, A. Paluszny, C. Pentland, Pore-scale imaging and modelling, *Adv. Water Resour.* 51 (2013) 197–216.
- [32] D.M. Jarvie, R.J. Hill, T.E. Ruble, R.M. Pollastro, Unconventional shale-gas systems: the Mississippian Barnett shale of north-central Texas as one model for thermogenic shale-gas assessment, *Am. Assoc. Petr. Geol.* B. 91 (2007) 475–499.
- [33] C. Fang, Y. Yafan, S. Shuyu, R. Qiao, Low salinity effect on the recovery of oil trapped by nanopores: A molecular dynamics study, *Fuel* 261 (2020) 116443:1–7.
- [34] M.S. Santos, L.F.M. Franco, M. Castier, I.G. Economou, Molecular dynamics simulation of n-Alkanes and CO<sub>2</sub> confined by calcite nanopores, *Energy Fuel* 32 (2018) 1934–1941.
- [35] M.M. Koleini, M.F. Mehraban, M.F. Ayatollahi, Effects of low salinity water on calcite/brine interface: A molecular dynamics simulation study, *Colloid. Surf. A* 537 (2018) 61–68.
- [36] G. Alonso, P. Gamallo, A. Mejía, R. Sayós, Assessing salt-surfactant synergistic effects on interfacial tension from molecular dynamics simulations, *J. Mol. Liq.* 299 (2020) 112233:1–11.
- [37] A.A. Ivanova, A.N. Cheremisin, A. Barifcani, S. Iglauer, C. Phan, Molecular insights in the temperature effect on adsorption of cationic surfactants at liquid/liquid interfaces, *J. Mol. Liq.* 299 (2020) 112104:1–9.
- [38] Y. Yanga, Z. Maa, F. Xiac, X. Lia, Adsorption behavior of oil-displacing surfactant at oil/water interface: Molecular simulation and experimental, *J. Wat. Proc. Eng.* 36 (2020) 101292:1–8.
- [39] M. Sedghi, M. Piri, L. Goual, Atomistic molecular dynamics simulations of crude oil/brine displacement in calcite mesopores, *Langmuir* 32 (2016) 3375–3384.
- [40] E.R. Remesal, J.A. Suárez, A.M. Márquez, J.F. Sanz, C. Rincón, J. Guitián, Molecular dynamics simulations of the role of salinity and temperature on the hydrocarbon/water interfacial tension, *Theor. Chem. Accounts* 136 (2017) 66:1–6.
- [41] A.M. Ali, N. Yahya, S. Qureshi, Interactions of ferro-nanoparticles (hematite and magnetite) with reservoir sandstone: implications for surface adsorption and interfacial tension reduction, *Pet. Sci.* 17 (2020) 1037–1055.
- [42] S. Tian, V. Erastova, S. Lu, H.C. Greenwell, T.R. Underwood, H. Xue, F. Zeng, G. Chen, C. Wu, R. Zhao, Understanding model crude oil component interactions on kaolinite silicate and aluminol surfaces: toward improved understanding of shale oil recovery, *Energy Fuel* 32 (2018) 1155–1165.
- [43] C. Bermúdez-Salguero, J. Gracia-Fadrique, Gibbs excess and the calculation of the absolute surface composition of liquid binary mixtures, *J. Phys. Chem. B* 119 (2015) 5598–5608.
- [44] J.G. Eberhart, The surface tension of binary liquid mixtures, *J. Phys. Chem.* 70 (1966) 1183–1186.
- [45] M. Salonen, J. Malila, I. Napari, A. Laaksonen, Evaluation of surface composition of surface active water-alcohol type mixtures: a comparison of semiempirical models, *J. Phys. Chem. B* 109 (2005) 3472–3479.
- [46] K.A. Connors, L. Wright, Dependence of surface tension on composition of binary aqueous-organic solutions, *Anal. Chem.* 61 (1989) 194–198.
- [47] A. Laaksonen, M. Kumala, An explicit cluster model for binary nuclei in water-alcohol systems, *J. Chem. Phys.* 95 (1991) 6745–6748.
- [48] S. Plimpton, Fast parallel algorithms for short-range molecular dynamics, *J. Comput. Phys.* 117 (1995) 1–19.
- [49] T. Schneider, E. Stoll, Molecular-dynamics study of a three-dimensional one-component model for distortive phase transitions, *Phys. Rev. B* 17 (1978) 1302–1322.
- [50] A.S. Nosé, A molecular dynamics method for simulations in the canonical ensemble, *Mol. Phys.* 52 (1984) 255–268.
- [51] H.J.C. Berendsen, J.P.M. Postma, W.F. van Gunsteren, A. DiNola, J.R. Haak, Molecular dynamics with coupling to an external bath, *J. Chem. Phys.* 81 (1984) 3684–3690.
- [52] W.G. Hoover, Constant-pressure equations of motion, *Phys. Rev. A* 34 (1986) 2499–2500.
- [53] R.W. Hockney, J.W. Eastwood, *Computer Simulation Using Particles*, Adam Hilger, New York, 1988.
- [54] J.G. Kirkwood, F.P. Buff, The statistical mechanical theory of surface tension, *J. Chem. Phys.* 17 (1949) 338–343.
- [55] L. Lundberg, O. Edholm, Dispersion corrections to the surface tension at planar surfaces, *J. Chem. Theory Comput.* 12 (2016) 4025–4032.
- [56] J. Alejandre, D.J. Tildesley, G.A. Chapela, Molecular dynamics simulation of the orthobaric densities and surface tension of water, *J. Chem. Phys.* 102 (1995) 4574–4583.
- [57] F.J. Martínez-Ruiz, B. Moreno-Ventas, F.J. Blas, Liquid-liquid interfacial properties of a symmetrical Lennard-Jones binary mixture, *J. Chem. Phys.* 143 (2015) 104706:1–11.
- [58] D. Duque, L.F. Vega, Some issues on the calculation of interfacial properties by molecular simulation, *J. Chem. Phys.* 121 (2004) 8611–8617.
- [59] A. Ghoufi, P. Malfreyt, D.J. Tildesley, Computer modelling of the surface tension of the gas-liquid and liquid-liquid interface, *Chem. Soc. Rev.* 45 (2016) 1387–1409.
- [60] J. Janacek, Long range corrections in inhomogeneous simulations, *J. Phys. Chem. B* 110 (2006) 6264–6269.
- [61] M.G. Martin, J.I. Siepmann, Transferable potentials for phase equilibria. 1. United-atom description of n-alkanes, *J. Phys. Chem. B* 102 (1998) 2569–2577.
- [62] J. Wang, R.M. Wolf, J.W. Caldwell, P.A. Kollman, D.A. Case, Development and testing of a general Amber force field, *J. Comput. Chem.* 15 (2004) 1157–1174.
- [63] N. Rai, J.I. Siepmann, Transferable potentials for phase equilibria. 9. Explicit hydrocarbon description of benzene and five-membered and six-membered heterocyclic aromatic compounds, *J. Phys. Chem. B* 111 (2007) 10790–10799.
- [64] H.J.C. Berendsen, J.P.M. Postma, W.F. van Gunsteren, J. Hermans, Interaction model for water in relation to protein hydration, in: B. Pullman (Ed.), *Intermolecular Forces*, Reidel, Dordrecht 1981, pp. 331–342.
- [65] H.J.C. Berendsen, J.R. Grigera, T.P. Straatsma, The missing term in effective pair potentials, *J. Phys. Chem.* 91 (1987) 6269–6271.
- [66] W.L. Jorgensen, J. Chandrasekhar, J.D. Madura, R.W. Impey, M.L. Klein, Comparison of simple potential functions for simulating liquid water, *J. Chem. Phys.* 79 (1983) 926–935.
- [67] W.L. Jorgensen, J.D. Madura, Temperature and size dependence for Monte Carlo simulations of TIP4P water, *Mol. Phys.* 56 (1985) 1381–1392.
- [68] J.L.F. Abascal, C. Vega, A general purpose model for the condensed phases of water: TIP4P/2005, *J. Chem. Phys.* 123 (2005) 234505:1–12.
- [69] J.P. Ryckaert, G. Cicotti, H.J.C. Berendsen, Numerical integration of the cartesian equations of motion of a system with constraints: molecular dynamics of n-alkanes, *J. Comput. Phys.* 23 (1977) 327–341.
- [70] S. Zeppieri, J. Rodríguez, A.L. López de Ramos, Interfacial tension of alkane + water systems, *J. Chem. Eng. Data* 46 (2001) 1086–1088.
- [71] H. Zhen, S. Ballinger, R. Pelton, E.D. Cranston, Surfactant-enhanced cellulose nanocrystal Pickering emulsions, *J. Colloid Interface Sci.* 439 (2015) 139–148.
- [72] REPSOL Internal Report.
- [73] A. Yeung, T. Dabros, J. Masliyah, Does equilibrium interfacial tension depend on method of measurement? *J. Colloid Interface Sci.* 208 (1998) 241–247.
- [74] K. Moran, A. Yeung, J. Masliyah, Measuring interfacial tensions of micrometer-sized droplets: a novel micromechanical technique, *Langmuir* 15 (1999) 8497–8504.
- [75] C. Herdes, Å. Ervik, A. Mejía, E.A. Müller, Prediction of the water/oil interfacial tension from molecular simulations using the coarse-grained SAFT-γ Mie force field, *Fluid Phase Equilib.* 476 (2018) 9–15.
- [76] K.D. Papavasileiou, O.A. Moulton, I.G. Economou, Predictions of water/oil interfacial tension at elevated temperatures and pressures: a molecular dynamics simulation study with biomolecular force fields, *Fluid Phase Equilib.* 476 (2018) 30–38.
- [77] H. Kim, D.J. Burgess, Prediction of interfacial tension between oil mixtures and water, *J. Colloid Interface Sci.* 241 (2001) 509–513.
- [78] I. Langmuir, The adsorption of gases on plane surfaces of glass, mica and platinum, *J. Am. Chem. Soc.* 40 (1918) 1361–1403.
- [79] A. Piñeiro, P. Brocos, A. Amigo, Extended Langmuir isotherm for binary liquid mixtures, *Langmuir* 17 (2001) 4261–4266.